ACS Catalysis

Research Article

pubs.acs.org/acscatalysis

Synthesis of Hierarchical Sn-MFI as Lewis Acid Catalysts for Isomerization of Cellulosic Sugars

Hong Je Cho, Paul Dornath, and Wei Fan*

Department of Chemical Engineering, University of Massachusetts, Amherst, Massachusetts 01003, United States

Supporting Information

ABSTRACT: Hierarchical stannosilicate molecular sieves with ordered mesoporosity and MFI topology (three dimensionally ordered mesoporous imprinted (3DOm-i) Sn-MFI) were successfully synthesized within the confined space of three dimensionally ordered mesoporous (3DOm) carbon by a seeded growth method. The obtained 3DOm-i Sn-MFI consisting of 30 nm spherical elements forming an opaline structure contains highly ordered mesopores ranging from 4 to 11 nm. Compared with conventional Sn-MFI, 3DOm-i Sn-MFI exhibits superior catalytic performance for the isomerization of cellulosic sugars. No diffusion limitation was observed for the isomerization of a triose sugar, dihydroxyacetone (DHA), into methyl lactate (ML). The presence of weak Brønsted acid in the 3DOm-i Sn-MFI catalyst facilitates the reaction by catalyzing the formation of an intermediate, pyruvaldehyde (PA). 3DOm-i Sn-MFI offers significant improvements for the isomerizations of C_5 and C_6 sugars, such as xylose and glucose, by greatly enhancing molecular transport. The reaction rate of xylose on 3DOm-i Sn-MFI is at least 20 times higher than that on conventional bulky sized Sn-MFI. The reaction rate for glucose is also enhanced by using 3DOm-i Sn-MFI, but to a lesser extent as compared with the reaction of xylose, possibly because glucose cannot diffuse into the 10-membered-ring pore of MFI, and the reaction is catalyzed only on the external surface of the Sn-MFI catalysts. Moreover, the combination of seeded growth with confined synthesis allows us to synthesize hierarchical Sn-MFI using commercially available carbon materials, such as carbon black and activated carbon, indicating that the synthesis strategy is a versatile and reliable method for tailoring the structure of hierarchical zeolites.

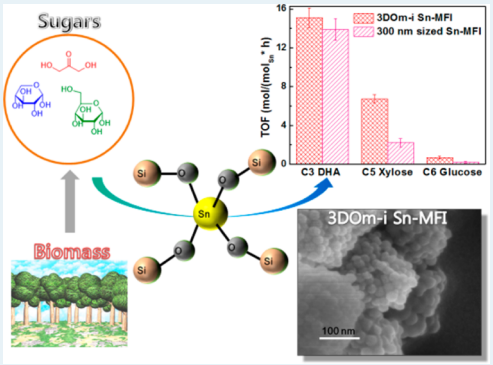

KEYWORDS: *hierarchical zeolite, Lewis acid catalyst, Sn-MFI, isomerization of cellulosic sugars, catalyst deactivation, biomass conversion*

1. INTRODUCTION

Zeolites have been widely used in petrochemical and biomass processing because of their distinct pore dimension, connectivity, framework and composition.[1,2] The microporous crystalline structures of zeolites provide excellent hydrothermal stability and molecular sieving capability for various catalytic reactions; however, the catalytic performance of zeolite catalysts can be hindered by slow molecular diffusion in their microporous structures, in particular, when bulky molecules are involved. Hierarchical zeolites consisting of mesoscale porosity superimposed on crystalline microporous structures offer a new class of porous materials exhibiting both molecular sieving capability and fast mass transport.[3−6] Fast molecular mass transport in hierarchical zeolites could facilitate molecules to access the active sites located within micropores and reduce the residence time of molecules in catalysts, leading to enhanced reaction rates and slower deactivation.[7−11]

Several approaches have been developed for the synthesis of hierarchical zeolites with intracrystalline mesopores, including desilication and dealumination of aluminosilicate zeolites, exfoliation and pillaring of layered zeolites, a supramolecular templating method, and a hard templating method.[12−21] Although a number of hierarchical zeolites have been synthesized using these methods so far, it is still a grand challenge to precisely control framework compositions and the size and shape of the formed mesopores. Recently, we reported that hierarchical zeolites with highly ordered mesoporous structures can be obtained by confining zeolite growth within three dimensionally ordered mesoporous (3DOm) carbon under hydrothermal conditions.[22] By combining seeded growth method with a confined synthesis method, hierarchical aluminosilicate zeolites with tunable mesoporosity and compositions were synthesized using the recipes developed for conventional hydrothermal synthesis of zeolites.[23] The synthesized hierarchical zeolites possess three dimensionally ordered mesoporous imprinted (3DOm-i) structure. The precisely controlled mesoporosity in 3DOm-i zeolites allows for the fundamental understanding of the effects of mesoporosity on the catalytic performance of this new class of porous materials.[24,25]

Increasing demand for energy and commodity chemicals has led to accelerated research efforts in the conversion of

Received: March 5, 2014
Revised: May 9, 2014
Published: May 12, 2014

renewable resource into chemicals and fuels for a sustainable economy. The processing of lignocellulosic biomass, an inexpensive, abundant and sustainable source of carbon, offers the promise of sustainable chemicals and carbon-neutral liquid transportation fuels.[26−30] Lewis acid catalysts play an important role for selectively activating functional groups of the organic molecules involved in biomass conversion. For example, Sn-containing molecular sieves and mesoporous silica materials show promising Lewis activity for catalyzing the isomerization of cellulosic sugars (C_3, C_5 and C_6 sugars),[26,31−34] the Meerwein−Ponndorf−Verley (MPV) reduction,[35−38] and several oxidation reactions, such as the Baeyer−Villiger oxidation and Meerwein−Ponndorf−Verley−Oppenauer oxidation.[38−41] Specifically, Sn-BEA, a molecular sieve with BEA topology containing tetrahedrally coordinated Sn, has shown high activity and selectivity for the isomerization of cellulosic sugars in an aqueous phase and formation of lactates from trioses in alcoholic media.[42,43] Stannosilicate with the MFI topology, Sn-MFI, has also been synthesized and used for carbohydrate-related reactions, exhibiting a promising catalytic activity for converting dihydroxyacetone (DHA) into lactic acid.[44] However, Sn-containing mesoporous silica catalysts, such as Sn-MCM-41 and Sn-SBA-15, exhibit a low catalytic activity for these reactions, probably because of the different local environment of Sn and the amorphous structure of the silica wall.[43,45]

Hierarchical Sn-containing molecular sieves consisting of active Lewis acid sites and tunable mesoporosity have promising implications for activating bulky molecules involved in the conversion of lignocellulosic biomass and fine chemical synthesis because the mesoporosity is able to facilitate molecules' access the catalytic active sites located on the external and internal surface of the catalysts. However, the synthesis of hierarchical Sn-containing zeolites is more challenging than their aluminosilicate analogues, mainly because of discrepancy in the reactivity of Sn and Si sources and the larger atomic size of Sn (Sn−O, ∼1.9 Å; Si−O, ∼1.7 Å). Sn-MFI nanosheets have been synthesized with an amphiphilic organic structure-directing agent.[46] Because of a high external surface area, this catalyst displays a much better catalytic activity than conventional Sn-MFI for the Baeyer−Villiger oxidation of cyclic ketones. Unfortunately, the catalytic activity of Sn-MFI nanosheets for the isomerization of cellulosic sugars was not explored, and the synthesis of the amphiphilic organic structure-directing agent is also costly. Moreover, the mesoporosity of Sn-MFI nanosheets, including mesopore size and structure, cannot be precisely controlled by this synthesis approach, which could limit the fundamental understanding of the effects of mesoporosity on the catalytic activity of the hierarchical catalysts. Herein, we demonstrated that the combination of a seeded growth method with confined synthesis is a versatile and reliable approach for the synthesis of hierarchical Sn-MFI catalysts. Hierarchical Sn-MFI catalysts with various mesoporous structures were synthesized from a variety of carbon templates and led to superior catalytic performances for the isomerization of cellulosic sugars, including DHA, xylose, and glucose in methanol.

2. EXPERIMENTAL SECTION

2.1. Catalyst Preparation. *Synthesis of 3DOm-i Sn-MFI.* A seeded growth method was applied for the confined synthesis of 3DOm-i Sn-MFI within a 3DOm carbon template. 3DOm carbon with a cage size of 35 nm was prepared according to a method reported in our previous literature.[47−49] The particle size of 3DOm carbon was 2−5 μm. A clear synthesis solution with a composition of 1 SiO_2/0.008 SnO_2/0.43 TPAOH/22.20 H_2O was prepared using a published recipe.[50] In a typical synthesis, 0.07 g of tin(IV) chloride pentahydrate ($SnCl_4 \cdot 5H_2O$, Alfa Aesar) was first mixed with 5.50 g of tetrapropylammonium hydroxide (40% TPAOH, Alfa Aesar) under stirring. Thereafter, 5.20 g of tetraethyl orthosilicate (TEOS, 98%, Alfa Aesar) was added into this mixture, followed by stirring for 30 min at room temperature. An additional 6.33 g of deionized water was added into the solution to reach the final composition. A transparent homogeneous solution was achieved after stirring for 24 h at room temperature. For the confined synthesis of Sn-MFI in the 3DOm carbon, 0.20 g of 3DOm carbon and 15 mL of the synthesis solution were mixed in a Teflon-lined autoclave and heated in an oven at 170 °C for 24 h to form Sn-MFI seeds. The solid product was recovered by filtration, followed by extensively washing with deionized water before mixing into a freshly prepared synthesis solution for the second cycle of the seeded growth. The seeded growth process was repeated three times. Finally, the as-made product was washed thoroughly by filtration with about 2 L of deionized water and dried in a convection oven at 100 °C overnight. The 3DOm carbon and the structure-directing agent (TPAOH) were removed from the product by calcination at 600 °C for 24 h in air.

Synthesis of Conventional Sn-MFI. Sn-MFI with a particle size of 300 nm denoted Sn-MFI_N was prepared using the same synthesis solution as 3DOm-i Sn-MFI. Crystallization was performed at 170 °C for 2 d. Large Sn-MFI with a particle size of 10 μm denoted Sn-MFI_L was synthesized by following published methods.[43,50] A 0.125 g portion of $SnCl_4 \cdot 5H_2O$ was premixed with 5.00 g of deionized water and slowly added to an ammonium fluoride (NH_4F, Alfa Aesar) aqueous solution made by dissolving 2.68 g of NH_4F in 12.50 g of deionized water. Subsequently, 4.90 g of tetrapropylammonium bromide (TPABr, Sigma-Aldrich) dissolved in 28.0 g of deionized water was added to this mixture. Finally, 4.3 g of fumed silica (Sigma-Aldrich) was added into this solution, and the mixture was stirred for 3 h at room temperature. The molar composition of the gel was 1 SiO_2/0.005 SnO_2/0.26 TPABr/1 NH_4F/35 H_2O. The crystallization was carried out at 200 °C for 6 d. The obtained Sn-MFI_L and Sn-MFI_N were washed with an excess amount of deionized water and dried at 100 °C overnight. Finally, the samples were calcined at 550 °C for 12 h in air.

2.2. Catalyst Characterization. Powder X-ray diffraction (XRD) patterns of the catalysts were recorded on an XRD diffractometer (X'Pert Pro, PANalytical) operated at an acceleration voltage of 45 kV and a current of 40 mA using Cu Kα radiation. The data were collected over a 2θ range of 4−40°. XRD patterns at low angle were collected on a pinhole small-angle X-ray scattering system (S-Max3000, Rigaku) using monochromatic Cu Kα radiation with a diameter of ∼0.4 mm. The SAXS intensity was measured by a two-dimensional gas-filled wire array detector at a distance of ∼1.5 m from the sample. The morphology of the products was examined by a scanning electron microscope (SEM, Magellan 400, FEI). Prior to the SEM measurement, the samples were coated with platinum. Both nitrogen (at 77 K) and argon (at 87 K) adsorption−desorption isotherms were measured by using an automated gas sorption analyzer (Autosorb iQ_2, Quantachrome) after the samples were degassed at 300 °C under

dx.doi.org/10.1021/cs500295u | ACS Catal. 2014, 4, 2029−2037

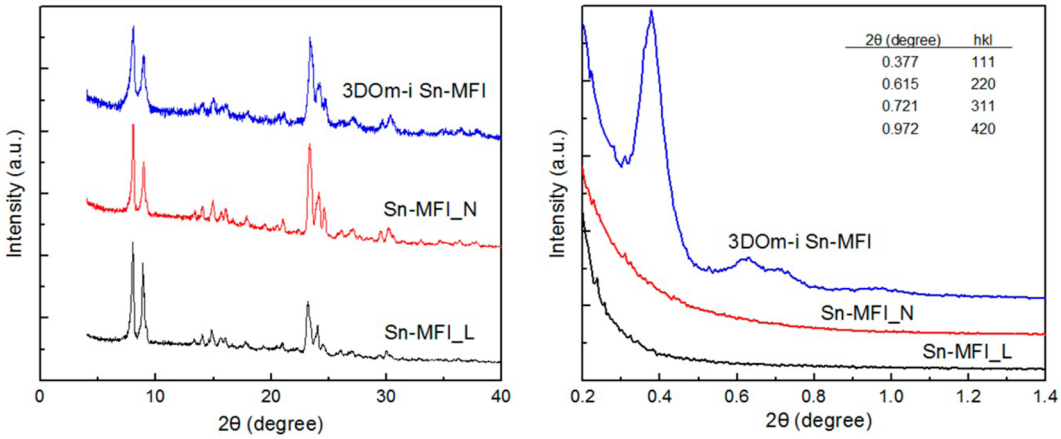

Figure 1. XRD (left) and SAXS (right) patterns of 3DOm-i Sn-MFI, Sn-MFI_N, and Sn-MFI_L samples.

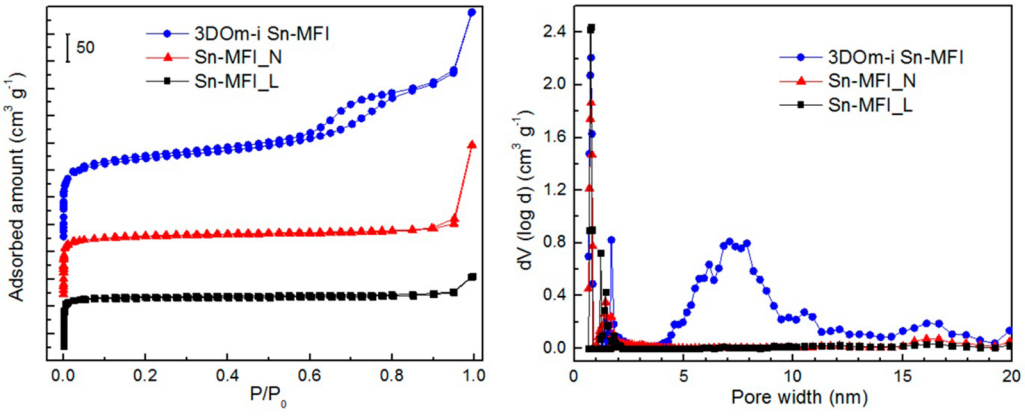

Figure 2. Argon adsorption−desorption isotherms (left) and pore size distributions using NLDFT (right) for 3DOm-i Sn-MFI, Sn-MFI_N, and Sn-MFI_L samples. Pore size distributions were calculated by using a NLDFT (nonlocal density functional theory) adsorption model, which describes Ar adsorbed in cylindrical pores (AsiQwin 1.02, Quantachrome).

vacuum. Elemental analysis was conducted on inductively coupled plasma optical emission spectroscopy (ICP-OES, iCap 6500 Dual view, Thermo Scientific). DRIFT-IR study was performed on EQUINOX 55 (Bruker) equipped with a MCT detector.[21,33] The samples were degassed at 550 °C for 1 h under He in a high-temperature reaction chamber containing a Praying Mantis diffuse reflection attachment (Harrick). Small aliquots of deuterated acetonitrile (CD_3CN) were carried by He and exposed to the sample at room temperature for 15 min. Prior to the characterization, the physically adsorbed acetonitrile was removed by flowing He at room temperature for 1 h. For FT-IR study on the samples with adsorbed pyridine, the spectra were collected at 120 °C after removing the weakly adsorbed pyridine at 250 °C under He for 1 h.

2.3. Catalytic Reaction. *Conversion of Dihydroxyacetone (DHA) and Pyruvaldehyde (PA) in Methanol (MeOH).* All chemicals used in the reactions were purchased from Sigma-Aldrich and used without further purification. In a typical experiment for converting DHA into methyl lactate (ML), 0.3125 mmol of DHA and 1.00 g of methanol were mixed within a 4 mL glass vial (Fisher Scientific). A corresponding amount of Sn-MFI catalysts with a DHA-to-Sn molar ratio of 127 was added to this mixture. The reactions were carried out at 70 °C. The same reaction conditions were also applied for pyruvaldehyde (PA, a 40 wt % aqueous solution).

Isomerization of Xylose (C_5 sugar) and Glucose (C_6 sugar) in MeOH. Xylose isomerization to xylulose and lyxose was performed in MeOH in a 4 mL glass vial. Typically, 1 g of xylose solution (1 wt % xylose) and 20 mg of catalyst were mixed in the reactor (xylose/Sn = 27). The glucose isomerization reaction was carried out under the same conditions over the Sn-MFI catalysts (glucose/Sn = 23).

All reactions were carried out for regular intervals on a temperature-controlled aluminum heating block with 1000 rpm stirring. After each reaction, the reactor was cooled in an ice bath for 20 min. The reactors were weighed before and after the reactions to ensure no leaking occurred. Naphthalene was used as an internal standard for all reactions.

2.4. Sample Analyses. DHA, ML, PA, and glyceraldehyde (GLA) were analyzed on an Agilent 6890 instrument equipped with an FID detector and a Restek RTX-VMS capillary column (30.0 m length, 0.25 mm id and 0.25 μm film thickness). Analyses of isomerization reactions of pentose (C_5) and hexose (C_6) sugars were carried out using liquid chromatography (LC, Shimadzu LC-20AT) with a BIO-RAD HPX-87H HPLC column operated at 30 °C. The mobile phase is 0.005 M sulfuric acid with a flow rate of 0.6 mL min^{-1}. The pentose and hexose sugars were quantified with a refractive index detector (RID-10A). In addition, a turnover frequency (TOF) value was calculated, which is defined as moles of product divided by moles of Sn per reaction time (h) when the product yield lies between 5 and 20%. On the basis of the ICP analysis (wt % of Sn in the catalyst), moles of Sn were calculated according to the reaction conditions.

dx.doi.org/10.1021/cs500295u | ACS Catal. 2014, 4, 2029−2037

Table 1. Textural Information of the Sn-MFI Samples from N_2 Adsorption−Desorption Isotherms and Composition Information

	BET surface area[a] ($m^2\ g^{-1}$)	micropore volume[b] ($cm^3\ g^{-1}$)	external surface area[b] ($m^2\ g^{-1}$)	total pore volume[c] ($cm^3\ g^{-1}$)	Si/Sn (initial gel)	Si/Sn (final product)[d]
Sn-MFI_L	330	0.116	62	0.185	200	256
Sn-MFI_N	386	0.117	149	0.293	125	135
3DOm-i Sn-MFI	459	0.119	191	0.402	125	133

[a]Calculated from a P/P_0 range of 0.05−0.25 using BET equation. [b]Calculated by the *t*-plot method. [c]Calculated from the amount adsorbed at P/P_0 = 0.975. [d]Determined by ICP-OES.

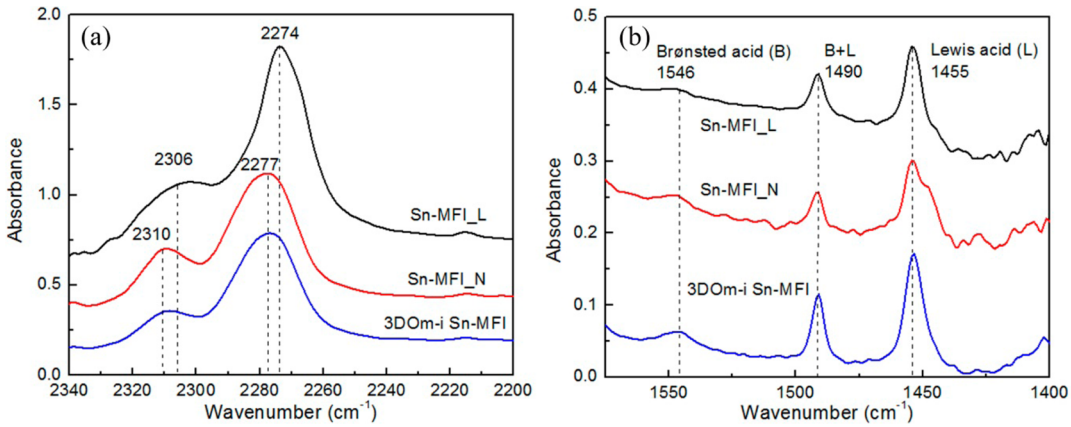

Figure 3. FT-IR spectra of 3DOm-i Sn-MFI, Sn-MFI_N, and Sn-MFI_L samples after adsorbing (a) deuterated acetonitrile and (b) pyridine.

3. RESULTS AND DISCUSSION

Figure 1 shows the XRD patterns of 3DOm-i Sn-MFI, Sn-MFI_N, and Sn-MFI_L synthesized in the study. Characteristic peaks corresponding to the MFI topology are observed for all three samples, indicating highly crystalline MFI zeolites have been synthesized without forming other impurity phases. The diffraction pattern of 3DOm-i Sn-MFI made from the seeded growth method exhibits broader peaks than the ones of Sn-MFI_N and Sn-MFI_L because of a small primary particle size. In the low-angle region of 2θ (0.2°−1.4°), four clear diffraction peaks were observed, revealing that the synthesized 3DOm-i Sn-MFI possesses a highly ordered mesoporous structure formed by a close-packing of primary particles.[21,49] These diffraction peaks can be indexed to the (111), (220), (311), and (420) planes according to a face-centered-cubic structure.[21] The size of unit cell calculated from the diffraction peaks is 41 nm, corresponding to a primary particle size of 29 nm, consistent with SEM observation shown in the section below.

Ar adsorption−desorption isotherms and pore size analyses of the three Sn-MFI samples are shown in Figure 2. The sharp adsorption uptake in the low relative pressure range, $P/P_0 < 0.1$, indicates the presence of microporosity in the samples. For 3DOm-i Sn-MFI, a gradual increase is observed in the relative pressure range from 0.5 to 0.8, corresponding to the imprinted mesoporous structure. The pore size distribution calculated using nonlocal density functional theory (NLDFT) further confirms the presence of dual micro- and mesoporosity in the 3DOm-i Sn-MFI sample with a micropore around 0.6 nm and a relatively narrow mesopore distribution from 4 to 11 nm. The BET surface area, micropore volume, external surface area, and total pore volume estimated by N_2 adsorption−desorption isotherms are summarized in Table 1. The micropore volumes for Sn-MFI_L, Sn-MFI_N, and 3DOm-i Sn-MFI were 0.116, 0.117, and 0.119 $cm^3\ g^{-1}$, respectively, clearly demonstrating that the MFI type crystal structure is well retained in the Sn-MFI samples. The BET surface area, external surface area, and total pore volume also increased with a reduction of the particle size of the Sn-MFI samples. The molar ratio of Si to Sn in each sample was quantified by an elemental analysis (Table 1).

The sole presence of the framework Sn, the Lewis acid site, in the 3DOm-i Sn-MFI sample was evident in the lack of H/D scrambling in glucose deuterated at the C-2 position (glucose-D2) and in the formation of fructose with the D-label retained at the C-1 position (Supporting Information Figure S1 and S2). This result is consistent with the previous study for Sn-BEA catalysts with framework Sn.[33] FT-IR and UV−vis spectra were used to further confirm the Lewis acidity and the presence of framework Sn in the samples. After deuterated acetonitrile (CD_3CN) vapors were exposed to Sn-MFI samples, the weakly adsorbed CD_3CN was removed from the solid samples by flowing He at room temperature for 1 h. As displayed in Figure 3, the FT-IR spectra of all three Sn-MFI samples showed bands at around 2275 cm^{-1}, consistent with the ν (C≡N) stretching mode of acetonitrile adsorbed on the silanol groups (Supporting Information Figure S3).[22,24,33] The bands near 2308 cm^{-1} are associated with the CD_3CN bound to isomorphously substituted Sn Lewis acid sites, in good agreement with previous reports.[41,43,51] The bands at both 2275 and 2308 cm^{-1} show a shift for the Sn-MFI_L synthesized in the presence of F^-, which might be related to changes in the packing structure of CD_3CN within the pores of the sample with different morphology and hydrophobicity, as suggested in the previous literature.[51] Moreover, diffuse-reflectance UV (DR-UV) spectra collected from the samples also suggested the presence of framework Sn (Supporting Information Figure S4).

In addition, the Lewis acidity of the catalysts is confirmed by FT-IR study of the pyridine saturated samples after a heat treatment at 250 °C for removing the weakly adsorbed pyridine. As shown in Figure 3b, Sn-MFI samples gave a strong absorption band at 1455 cm^{-1}, corresponding to the

dx.doi.org/10.1021/cs500295u | ACS Catal. 2014, 4, 2029−2037

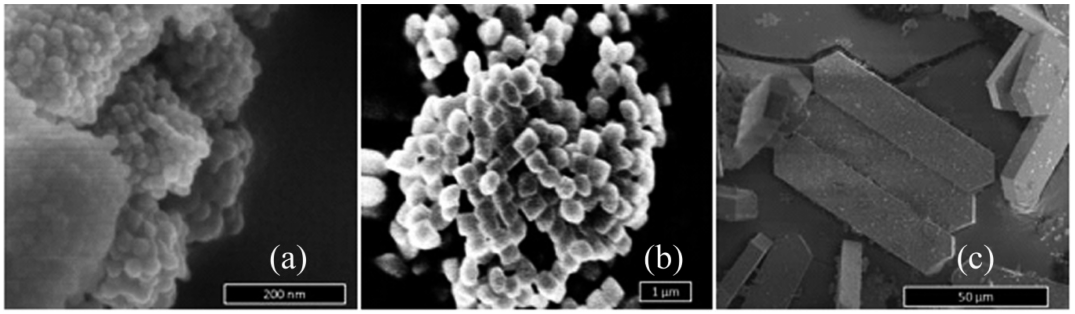

Figure 4. SEM images of (a) 3DOm-i Sn-MFI, (b) Sn-MFI_N, and (c) Sn-MFI_L.

Scheme 1. Reaction Pathway for the Conversion of Dihydroxyacetone (DHA) or Glyceraldehyde (GLA) in Methanol (MeOH) into Either Methyl Lactate (ML) or Pyruvaldehyde Dimethylacetal (PADA)

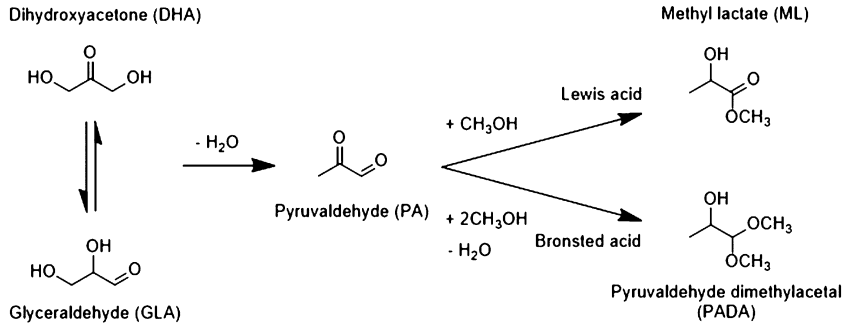

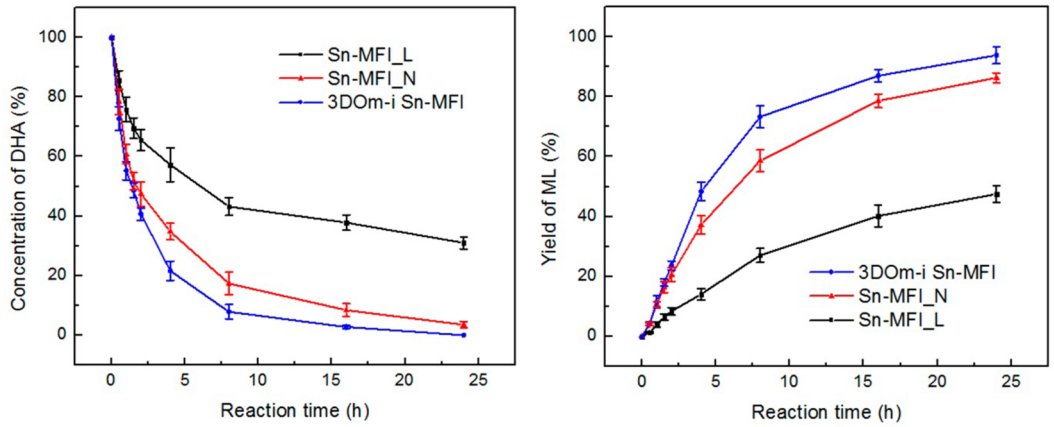

Figure 5. Reaction profiles for the conversion of DHA to ML on different Sn-MFI catalysts. The error bars in the figures are from three repeated reactions.

pyridine molecules bound with Lewis acidic Sn site.[45,52] Owing to its Lewis acidity, the Sn site is able to adsorb pyridine at 250 °C, similar to other Sn-containing molecular sieves.[53] A very weak absorption band at 1546 cm^{-1} associated with Brønsted acid was also observed in the spectra.[45,52] All the four characterizations performed on the Sn-MFI samples clearly indicate that the prepared samples possess mainly framework-coordinated Sn atoms, which are responsible for the Lewis acid sites. A small number of Brønsted acid sites might also be present in the samples as a result of silanol defects.

The morphology of synthesized samples was characterized by SEM (Figure 4). As shown in Figure 4c, Sn-MFI_L synthesized in fluoride media shows a large particle size, approximately 60 μm × 15 μm × 3 μm, and a typical coffin shape of the MFI crystal. Sn-MFI_N sample was synthesized in the presence of hydroxide ions (OH^-) and has a particle size from 250 to 350 nm (Figure 4b). Different from conventional zeolites with MFI topology, 3DOm-i Sn-MFI with a particle size of around 1 μm is composed of spherical primary particles having a close-packing arrangement. The primary particle size is around 30 nm, consistent with the value calculated from the low-angle X-ray diffraction measurement, revealing that a confined growth in the 3DOm carbon has been achieved in this synthesis.

The catalytic activity of the synthesized Sn-MFI samples was systemically evaluated using the isomerizations of C_3, C_5 and C_6 sugars in MeOH. Scheme 1 illustrates the proposed reaction pathway for the conversion of triose sugars, DHA and GLA, in the presence of MeOH. PA, an initial intermediate formed by the dehydration of DHA or GLA, can be converted to either ML by Lewis acids or pyruvaldehyde dimethylacetal (PADA) by Brønsted acids.[26,52] It has been shown that Sn-containing materials as highly active Lewis acid catalysts can activate the carbonyl and hydroxyl groups in PA, facilitating an intramolecular hydride shift similar to the MPV reactions catalyzed

dx.doi.org/10.1021/cs500295u | ACS Catal. 2014, 4, 2029−2037

by Lewis acids.[54] On the other hand, weak Brønsted acid sites can promote the initial dehydration step for producing PA from DHA or GLA, whereas strong Brønsted acids should be avoided because they can further catalyze the formed PA to produce PADA instead of ML in the second step of the reaction pathway.[45,55]

For all three Sn-MFI samples, no PADA was detected during the reaction starting from DHA in MeOH at 70 °C, indicating that the Sn-MFI catalysts do not have strong Brønsted acidity. Figure 5 reveals that the 3DOm-i Sn-MFI catalyst produces the highest yield of ML. After 24 h, a 93.8% yield of ML was achieved for the 3DOm-i Sn-MFI catalyst, whereas the yields of ML for Sn-MFI_N and Sn-MFI_L were 86.3% and 47.5%, respectively. As shown in Figure 6, 3DOm-i Sn-MFI and Sn-MFI_N gave a higher initial reactivity (TOF = 15.1 for 3DOm-i Sn-MFI and TOF = 13.9 for Sn-MFI_N) than Sn-MFI_L (TOF = 4.3) under the reaction conditions. Since it has been known that weak Brønsted acidity from silanol groups associated with the surface terminal groups and defects in zeolites can catalyze the dehydration reaction from DHA to PA,[56−58] it is anticipated that different activities of the Sn-MFI catalysts might be due to the number of weak Brønsted acid sites located in these catalysts.

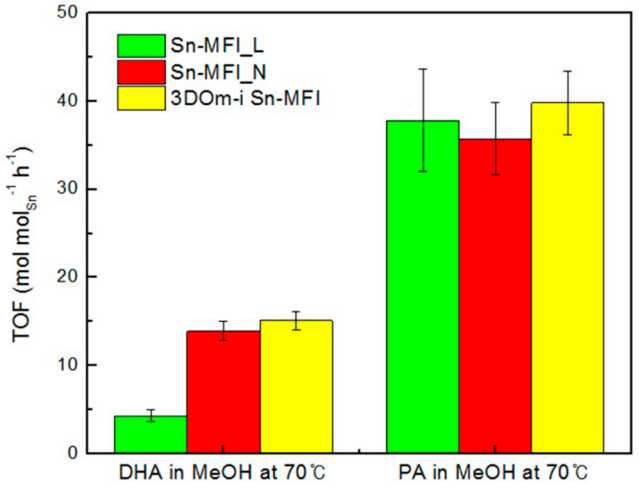

Figure 6. Initial catalytic activities of Sn-MFI catalysts for the conversions of DHA and PA in the presence of MeOH. The error bars in the figures are from three repeated reactions.

Figure 7 shows FT-IR spectra collected from the samples after removing the adsorbed water by degassing at 550 °C. In this figure, the band at 3745 cm^{-1} comes from the silanol groups on the external surface of the samples. The features at 3726 and 3700 cm^{-1} can be assigned to the silanol groups located inside the micropores of zeolites.[59,60] The band around 3500 cm^{-1} is ascribed to silanol nests that occur at extended defects.[59] Sn-MFI_L shows weaker absorption for all three types of Si−OH groups and defects than Sn-MFI_N and 3DOm-i Sn-MFI, clearly indicating the use of F$^-$ in the synthesis led to fewer defects and lower external surface area. Notably, the 3DOm-i Sn-MFI exhibits the highest concentration of Si−OH groups among the measured samples. It is very likely the high concentration of weak Brønsted acids associated with silanol groups resulted in the superior catalytic performance of the 3DOm-i Sn-MFI catalyst for the conversion of DHA into ML (Supporting Information Figure S5). In addition, product distributions with reaction time for the conversion of DHA into ML (Supporting Information Figure S6) reveal that the concentration of intermediate PA remains lower than the one of DHA or GLA during the whole reaction, implying that the dehydration reaction from DHA to PA is a rate-limiting step for the conversion of DHA into ML.

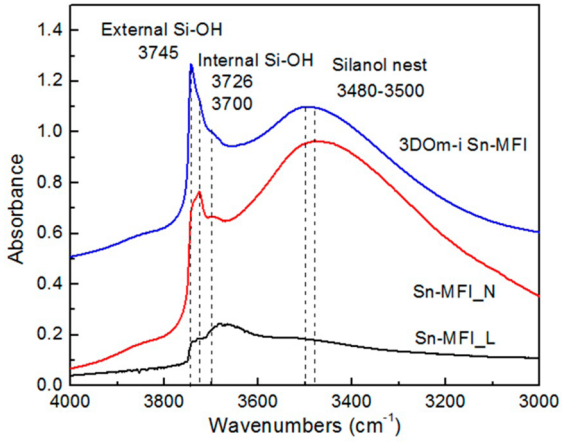

Figure 7. FT-IR spectra in the OH-stretch region (3800−3000 cm^{-1}) of the Sn-MFI catalysts.

Because the rate-limiting step for the reaction from DHA to ML is the first step, the dehydration reaction, the catalytic performance of the Sn-MFI catalysts is determined by the number of weak Brønsted acids in the catalysts. To further understand the effects of mass transport on the catalytic performance of the Sn-MFI catalysts, PA, the product from the dehydration of DHA, was used as a reactant to produce ML over the catalysts. In the reaction, PA is directly converted into ML over the Lewis acid sites of the Sn-MFI catalysts through an intramolecular 1,2 hydride shift. For the reaction, all three Sn-MFI catalysts possess similar initial activities, as shown in Figure 6, regardless of the crystal size or mesoporosity of the catalysts. The result strongly suggests that there is no diffusion limitation in the isomerization of PA for the tested Sn-MFI catalysts. In addition, because the dehydration is the rate-limiting step in the two-step reaction from DHA to ML, the catalytic performance of Sn-MFI catalysts for the conversion of DHA to ML can be optimized by further enhancing the dehydration reaction through tailoring the number of defects and silanol groups on the catalysts.

Furthermore, the isomerizations of pentose (C_5) and hexose (C_6) sugars in MeOH have been tested over the three Sn-MFI catalysts. Xylose, which is the most abundantly available pentose sugar in hemicellulose, undergoes isomerization to generate xylulose and lyxose via an intramolecular 1,2 hydride shift.[31] On the other hand, when glucose is chosen as a starting substrate, the resulting products are fructose and mannose.[32] The test results are expressed in terms of TOF, as depicted in Figure 8. In both reactions, Sn-MFI_L was nearly inactive because of the large crystal size and small external surface area. 3DOm-i Sn-MFI results in a remarkable catalytic performance for the reactions, showing at least 3-fold higher activity than Sn-MFI_N. In the case of xylose isomerization, the enhanced reaction rate on 3DOm-i Sn-MFI can be explained by the reduced diffusion limitation of xylose within the hierarchically structured catalyst. The ten-membered ring of MFI structure is composed of straight and sinusoidal channels, depending on the crystal orientation.[61,62] As a matter of fact, it has been

dx.doi.org/10.1021/cs500295u | ACS Catal. 2014, 4, 2029−2037

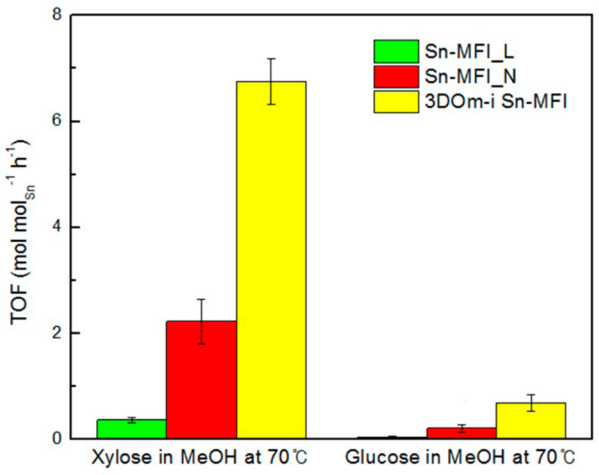

Figure 8. Initial catalytic activities of Sn-MFI catalysts for isomerizations of xylose and glucose. The error bars in the figures are from three repeated reactions.

suggested that the molecules smaller than 0.63 nm should be able to sufficiently fit into the micropores of an MFI crystal.[63,64] Because of the slightly larger molecular size of xylose (0.65 nm, Stokes diameter; 0.68 nm, equivalent molar diameter) compared with the pore size of the MFI crystal (0.63 nm),[65] diffusion limitation might become critical for the reaction, giving rise to more pronounced differences in the performances between the hierarchical, 300 nm, and bulky Sn-MFI catalysts.

For glucose (C_6 sugar) isomerization, all TOF values appear to be very low, although better activity was observed for 3DOm-i Sn-MFI zeolite. Taking into account the kinetic diameter of glucose (0.86 nm),[64] it is quite challenging for glucose to diffuse into the micropores of the MFI catalyst. This isomerization reaction for glucose is very likely to occur only on the exterior surface of the Sn-MFI catalysts. These results are in good agreement with earlier studies[32,44] showing that Ti- or Sn-MFI zeolites are not active for the glucose isomerization because glucose is too large to enter the micropore of the MFI crystal. The TOF values for the three Lewis acid-catalyzed reactions are summarized in Table 2. When the substrate changes from C_3 to C_5, the Sn-MFI catalysts begin to show different catalytic activities because of the diffusion limitation of xylose compared with C_3 sugars. For the reaction of an even larger sugar, glucose, it seems that the reaction happens only on the exterior surfaces of the catalysts because glucose is much larger than the MFI pore dimensions. The results clearly suggest that 3DOm-i Sn-MFI provides a superior catalytic performance for cellulosic sugar isomerizations compared with conventional Sn-MFI. The enhanced catalytic activity is very likely because the mesopores imposed in the zeolites can considerably enhance the molecular diffusion of the bulky molecules.

Table 2. Summary of TOF for Three Lewis Acid-Catalyzed Reactions

	TOF[a] (h^{-1})		
catalyst	PA in MeOH	Xylose in MeOH	Glucose in MeOH
Sn-MFI_L	37.8 (±5.8)	0.37 (±0.05)	0.05 (±0.01)
Sn-MFI_N	35.7 (±4.1)	2.23 (±0.42)	0.21 (±0.07)
3DOm-i Sn-MFI	39.8 (±3.6)	6.76 (±0.43)	0.69 (±0.15)

[a]95% confidence interval in parentheses.

In addition to enhanced reaction rates, hierarchical zeolites with mesopores can also improve the catalyst lifetime and reduce catalyst deactivation in various reactions.[9,11,14] During the course of triose isomerization, recent studies have reported that heterogeneous catalysts are deactivated as a result of the coke accumulation onto the catalyst surface.[42,45,52] To gain insights into the effect of mesoporosity on catalyst deactivation, high conversion results from PA to ML were collected over the prepared Sn-MFI catalysts and are presented in Figure 9. At the beginning of the reaction, the reaction rate for all Sn-MFI catalysts was the same as shown earlier. With the further progress of the reaction, the catalytic activities of the catalysts exhibited distinct differences. Specifically, 3DOm-i Sn-MFI gave a 94.1% yield of ML after 10 h, whereas 83.4% and 74.8% yields of ML were obtained for Sn-MFI_N and Sn-MFI_L, respectively. Because an excess amount of methanol was used, the isomerization reaction can be approximated as pseudo-first-order in the limiting reactant PA. Plots of $-\ln(1 - x)$ against a reaction time (x is the product yield for this reaction) suggest that the reaction over 3DOm-i Sn-MFI is in a good agreement with the pseudo-first-order approximation; however, the reactions over Sn-MFI_N and Sn-MFI_L show evident discrepancy from the approximation at high conversion (Supporting Information Figure S7). This is a strong indication that the catalyst deactivation occurred slowly on the 3DOm-i Sn-MFI catalyst because the highly interconnected mesoporous structures allow facile molecular diffusion into and out of the micropores of the catalyst. Consequently, it was inferred that the Sn-MFI catalyst with hierarchical porosity shows slower deactivation, leading to better catalytic performances.

The feasibility of the seeded growth method for the synthesis of hierarchical Sn-MFI catalysts has been further explored using other commercially available carbon materials. With the same approach used in the 3DOm-i Sn-MFI synthesis, hierarchical Sn-MFI was fabricated with carbon black BP2000 and activated carbon Norit SX Ultra, respectively. Cumulative pore volumes and pore size distributions estimated from NLDFT for the samples are presented in Figure S8 (Supporting Information). In these plots, hierarchical Sn-MFI materials synthesized within commercial carbon templates exhibit mesopores with a broad range from 3 to 20 nm. This is probably caused by disorderly interconnected carbon nanoparticles in the commercial carbons. Figure S9 (Supporting Information) displays a SEM image of Sn-MFI synthesized within carbon black BP2000. The Sn-MFI crystals seem to nucleate within the pores of the carbon template and grow up to outside of the carbon template during the repeated seeded growth process, leading to encapsulation of the carbon nanoparticles within the formed crystals. The results clearly indicate that the characteristics of hierarchical zeolite catalysts synthesized by the seeded growth method can be easily tailored by controlling the porous structures (e.g., pore size and interconnectivity) of the carbon templates.

4. CONCLUSIONS

Hierarchical Sn-MFI catalysts with different mesoporous structures were successfully synthesized within the confined space of 3DOm carbon and commercial carbon templates by a seeded growth approach. Highly crystalline 3DOm-i Sn-MFI with tetrahedrally coordinated framework Sn exhibits ordered mesopores from 4 to 11 nm. The imposed mesoporosity can be

dx.doi.org/10.1021/cs500295u | ACS Catal. 2014, 4, 2029−2037

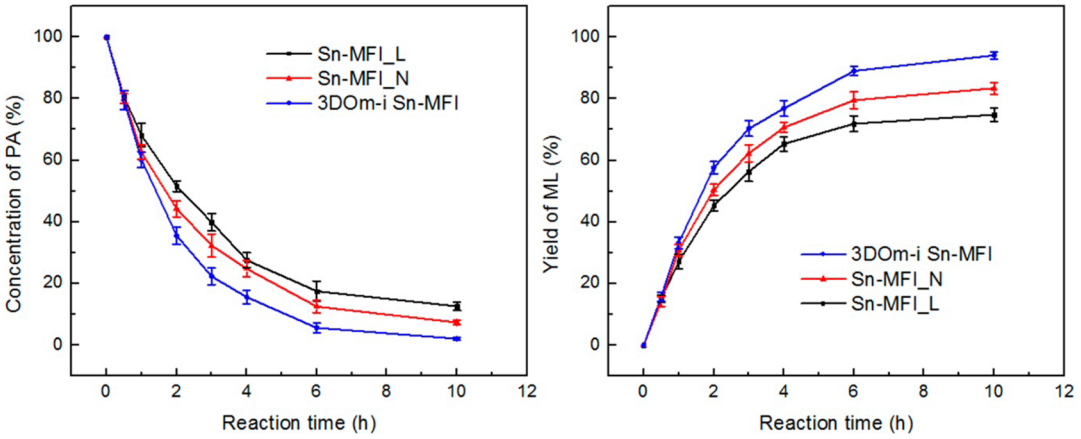

Figure 9. Reaction profiles for the conversion of PA to ML using different Sn-MFI catalysts. The error bars in the figures are from three repeated reactions.

easily tailored by using carbon templates with different porosities. This hierarchical catalyst showed superior catalytic performance for the isomerization of cellulosic sugars (C_3, C_5 and C_6 sugars). No diffusion limitation was observed for the conversion of DHA to ML on the Sn-MFI catalysts. The rate-limiting step for the reaction is the dehydration (1st step) of the triose sugar, DHA, which can be catalyzed by the weak Brønsted acid sites arising from silanol defects in the catalysts. In the case of converting bulky molecules, such as pentose and hexose sugars, 3DOm-i Sn-MFI displayed a 20-times-higher catalytic activity than conventional bulky Sn-MFI catalyst. Nevertheless, because the size of glucose is much larger than the MFI pore dimensions, glucose might encounter a difficulty to enter the pores of Sn-MFI samples, leading to the isomerization occurring only on the external surface of the catalysts. On the basis of these results, it is concluded that 3DOm-i Sn-MFI catalysts with multilength scale porosity can provide large molecules with easy accessibility to the active Lewis acid sites located on the external and internal surface of the catalysts. Furthermore, commercially available carbon materials can be also used to synthesize hierarchical Sn-MFI using the method developed in the study, indicating the combination of seeded growth with confined synthesis is a versatile and reliable method for the control of structure of hierarchical zeolites.

■ ASSOCIATED CONTENT

Supporting Information

Further details of ^{1}H NMR and ^{13}C NMR, FT-IR, UV−vis, reaction data, N_2 sorption isotherms and SEM are given in Figures S1−S9. This material is available free of charge via the Internet at http://pubs.acs.org.

■ AUTHOR INFORMATION

Corresponding Author

*Phone: (+1) 413-545-1750. Fax: (+1) 413-545-1647. E-mail: wfan@ecs.umass.edu.

Notes

The authors declare no competing financial interest.

■ ACKNOWLEDGMENTS

Hong Je Cho was supported by the start-up fund from University of Massachusetts, Amherst. Wei Fan and Paul Dornath were supported by the Catalysis Center for Energy Innovation, an Energy Frontier Research Center funded by the U.S. Department of Energy, Office of Science, and Office of Basic Energy Sciences under Award No. DE-SC0001004.

■ REFERENCES

(1) Corma, A. *Chem. Rev.* **1997**, *97*, 2373−2419.
(2) Davis, M. E. *Nature* **2002**, *417*, 813−821.
(3) Hartmann, M. *Angew. Chem., Int. Ed.* **2004**, *43*, 5880−5882.
(4) Cejka, J.; Mintova, S. *Catal. Rev.-Sci. Eng.* **2007**, *49*, 457−509.
(5) Egeblad, K.; Christensen, C. H.; Kustova, M. *Chem. Mater.* **2008**, *20*, 946−960.
(6) Perez-Ramirez, J.; Christensen, C. H.; Egeblad, K.; Groen, J. C. *Chem. Soc. Rev.* **2008**, *37*, 2530−2542.
(7) Zhang, X. Y.; Liu, D. X.; Xu, D. D.; Asahina, S.; Cychosz, K. A.; Agrawal, K. V.; Al Wahedi, Y.; Bhan, A.; Al Hashimi, S.; Terasaki, O.; Thommes, M.; Tsapatsis, M. *Science* **2012**, *336*, 1684−1687.
(8) Na, K.; Jo, C.; Kim, J.; Cho, K.; Jung, J.; Seo, Y.; Messinger, R. J.; Chmelka, B. F.; Ryoo, R. *Science* **2011**, *333*, 328−332.
(9) Shetti, V. N.; Kim, J.; Srivastava, R.; Choi, M.; Ryoo, R. *J. Catal.* **2008**, *254*, 296−303.
(10) Choi, M.; Cho, H. S.; Srivastava, R.; Venkatesan, C.; Choi, D. H.; Ryoo, R. *Nat. Mater.* **2006**, *5*, 718−723.
(11) Choi, M.; Na, K.; Kim, J.; Sakamoto, Y.; Terasaki, O.; Ryoo, R. *Nature* **2009**, *461*, 246−249.
(12) Groen, J. C.; Zhu, W. D.; Brouwer, S.; Huynink, S. J.; Kapteijn, F.; Moulijn, J. A.; Perez-Ramirez, J. *J. Am. Chem. Soc.* **2007**, *129*, 355−360.
(13) Wang, Q. L.; Giannetto, G.; Torrealba, M.; Perot, G.; Kappenstein, C.; Guisnet, M. *J. Catal.* **1991**, *130*, 459−470.
(14) Srivastava, R.; Choi, M.; Ryoo, R. *Chem. Commun.* **2006**, 4489−4491.
(15) Verboekend, D.; Perez-Ramirez, J. *Catal. Sci. Technol.* **2011**, *1*, 879−890.
(16) Corma, A.; Fornes, V.; Pergher, S. B.; Maesen, T. L. M.; Buglass, J. G. *Nature* **1998**, *396*, 353−356.
(17) Wu, P.; Ruan, J. F.; Wang, L. L.; Wu, L. L.; Wang, Y.; Liu, Y. M.; Fan, W. B.; He, M. Y.; Terasaki, O.; Tatsumi, T. *J. Am. Chem. Soc.* **2008**, *130*, 8178−8187.
(18) Tao, Y.; Kanoh, H.; Kaneko, K. *J. Am. Chem. Soc.* **2003**, *125*, 6044−6045.
(19) Tao, Y.; Kanoh, H.; Kaneko, K. *Langmuir* **2004**, *21*, 504−507.
(20) Tao, Y. S.; Kanoh, H.; Abrams, L.; Kaneko, K. *Chem. Rev.* **2006**, *106*, 896−910.
(21) Fan, W.; Snyder, M. A.; Kumar, S.; Lee, P. S.; Yoo, W. C.; McCormick, A. V.; Penn, R. L.; Stein, A.; Tsapatsis, M. *Nat. Mater.* **2008**, *7*, 984−991.
(22) Chen, H. Y.; Wydra, J.; Zhang, X. Y.; Lee, P. S.; Wang, Z. P.; Fan, W.; Tsapatsis, M. *J. Am. Chem. Soc.* **2011**, *133*, 12390−12393.

(23) Wang, Z.; Dornath, P.; Chang, C.-C.; Chen, H.; Fan, W. *Microporous Mesoporous Mater.* **2013**, *181*, 8−16.
(24) Chang, C.-C.; Teixeira, A. R.; Li, C.; Dauenhauer, P. J.; Fan, W. *Langmuir* **2013**, *29*, 13943−13950.
(25) Teixeira, A. R.; Chang, C.-C.; Coogan, T.; Kendall, R.; Fan, W.; Dauenhauer, P. J. *J. Phys. Chem. C* **2013**, *117*, 25545−25555.
(26) Holm, M. S.; Saravanamurugan, S.; Taarning, E. *Science* **2010**, *328*, 602−605.
(27) Huber, G. W.; Iborra, S.; Corma, A. *Chem. Rev.* **2006**, *106*, 4044−4098.
(28) Chheda, J. N.; Huber, G. W.; Dumesic, J. A. *Angew. Chem., Int. Ed.* **2007**, *46*, 7164−7183.
(29) Huber, G. W.; Corma, A. *Angew. Chem., Int. Ed.* **2007**, *46*, 7184−7201.
(30) Lin, Y. C.; Huber, G. W. *Energy Environ. Sci.* **2009**, *2*, 68−80.
(31) Choudhary, V.; Pinar, A. B.; Sandler, S. I.; Vlachos, D. G.; Lobo, R. F. *ACS Catal.* **2011**, *1*, 1724−1728.
(32) Moliner, M.; Roman-Leshkov, Y.; Davis, M. E. *Proc. Natl. Acad. Sci. U.S.A.* **2010**, *107*, 6164−6168.
(33) Román-Leshkov, Y.; Moliner, M.; Labinger, J. A.; Davis, M. E. *Angew. Chem., Int. Ed.* **2010**, *49*, 8954−8957.
(34) Gounder, R.; Davis, M. E. *AIChE J.* **2013**, *59*, 3349−3358.
(35) Corma, A.; Domine, M. E.; Nemeth, L.; Valencia, S. *J. Am. Chem. Soc.* **2002**, *124*, 3194−3195.
(36) Corma, A.; Domine, M. E.; Valencia, S. *J. Catal.* **2003**, *215*, 294−304.
(37) Boronat, M.; Corma, A.; Renz, M. *J. Phys. Chem. B* **2006**, *110*, 21168−21174.
(38) Boronat, M.; Corma, A.; Renz, M.; Viruela, P. M. *Chem.—Eur. J.* **2006**, *12*, 7067−7077.
(39) Corma, A.; Nemeth, L. T.; Renz, M.; Valencia, S. *Nature* **2001**, *412*, 423−425.
(40) Boronat, M.; Concepción, P.; Corma, A.; Renz, M.; Valencia, S. *J. Catal.* **2005**, *234*, 111−118.
(41) Boronat, M.; Concepcion, P.; Corma, A.; Navarro, M. T.; Renz, M.; Valencia, S. *Phys. Chem. Chem. Phys.* **2009**, *11*, 2876−2884.
(42) Taarning, E.; Saravanamurugan, S.; Holm, M. S.; Xiong, J. M.; West, R. M.; Christensen, C. H. *ChemSusChem* **2009**, *2*, 625−627.
(43) Osmundsen, C. M.; Holm, M. S.; Dahl, S.; Taarning, E. *Proc. R. Soc. A* **2012**, *468*, 2000−2016.
(44) Lew, C. M.; Rajabbeigi, N.; Tsapatsis, M. *Microporous Mesoporous Mater.* **2012**, *153*, 55−58.
(45) Li, L.; Stroobants, C.; Lin, K. F.; Jacobs, P. A.; Sels, B. F.; Pescarmona, P. P. *Green Chem.* **2011**, *13*, 1175−1181.
(46) Luo, H. Y.; Bui, L.; Gunther, W. R.; Min, E.; Roman-Leshkoy, Y. *ACS Catal.* **2012**, *2*, 2695−2699.
(47) Davis, T. M.; Snyder, M. A.; Krohn, J. E.; Tsapatsis, M. *Chem. Mater.* **2006**, *18*, 5814−5816.
(48) Snyder, M. A.; Lee, J. A.; Davis, T. M.; Scriven, L. E.; Tsapatsis, M. *Langmuir* **2007**, *23*, 9924−9928.
(49) Yokoi, T.; Sakamoto, Y.; Terasaki, O.; Kubota, Y.; Okubo, T.; Tatsumi, T. *J. Am. Chem. Soc.* **2006**, *128*, 13664−13665.
(50) Mal, N. K.; Ramaswamy, V.; Rajamohanan, P. R.; Ramaswamy, A. V. *Microporous Mater.* **1997**, *12*, 331−340.
(51) Roy, S.; Bakhmutsky, K.; Mahmoud, E.; Lobo, R. F.; Gorte, R. J. *ACS Catal.* **2013**, *3*, 573−580.
(52) West, R. M.; Holm, M. S.; Saravanamurugan, S.; Xiong, J. M.; Beversdorf, Z.; Taarning, E.; Christensen, C. H. *J. Catal.* **2010**, *269*, 122−130.
(53) Chang, C. C.; Wang, Z. P.; Dornath, P.; Cho, H. J.; Fan, W. *RSC Adv.* **2012**, *2*, 10475−10477.
(54) Román-Leshkov, Y.; Davis, M. E. *ACS Catal.* **2011**, *1*, 1566−1580.
(55) Pescarmona, P. P.; Janssen, K. P. F.; Delaet, C.; Stroobants, C.; Houthoofd, K.; Philippaerts, A.; De Jonghe, C.; Paul, J. S.; Jacobs, P. A.; Sels, B. F. *Green Chem.* **2010**, *12*, 1083−1089.
(56) Bordiga, S.; Roggero, I.; Ugliengo, P.; Zecchina, A.; Bolis, V.; Artioli, G.; Buzzoni, R.; Marra, G.; Rivetti, F.; Spano, G.; Lamberti, C. *J. Chem. Soc., Dalton Trans.* **2000**, 3921−3929.
(57) Corma, A.; Rey, F.; Rius, J.; Sabater, M. J.; Valencia, S. *Nature* **2004**, *431*, 287−290.
(58) Trzpit, M.; Soulard, M.; Patarin, J.; Desbiens, N.; Cailliez, F.; Boutin, A.; Demachy, I.; Fuchs, A. H. *Langmuir* **2007**, *23*, 10131−10139.
(59) Barbera, K.; Bonino, F.; Bordiga, S.; Janssens, T. V. W.; Beato, P. *J. Catal.* **2011**, *280*, 196−205.
(60) Trombetta, M.; Armaroli, T.; Alejandre, A. G.; Solis, J. R.; Busca, G. *Appl. Catal., A* **2000**, *192*, 125−136.
(61) Jae, J.; Tompsett, G. A.; Foster, A. J.; Hammond, K. D.; Auerbach, S. M.; Lobo, R. F.; Huber, G. W. *J. Catal.* **2011**, *279*, 257−268.
(62) Yu, M.; Wyss, J. C.; Noble, R. D.; Falconer, J. L. *Microporous Mesoporous Mater.* **2008**, *111*, 24−31.
(63) *International Zeolite Association database of zeolite structures*, http://www.iza-structure.org/databases.
(64) Li, S. G.; Tuan, V. A.; Falconer, J. L.; Noble, R. D. *J. Membr. Sci.* **2001**, *191*, 53−59.
(65) Sjoman, E.; Manttari, M.; Nystrom, M.; Koivikko, H.; Heikkila, H. *J. Membr. Sci.* **2007**, *292*, 106−115.